Available online at www.sciencedirect.com
SCIENCE DIRECT®
Journal of Solid State Chemistry 176 (2003) 221–233
JOURNAL OF SOLID STATE CHEMISTRY
http://elsevier.com/locate/jssc

Double ($n = 2$) and triple ($n = 3$) $[M_4Bi_{2n-2}O_{2n}]^{x+}$ polycationic ribbons in the new $Bi_{\sim 3}Cd_{\sim 3.72}M_{\sim 1.28}O_5(PO_4)_3$ oxyphosphate (M = Co, Cu, Zn)

Marie Colmont,[a] Marielle Huvé,[a] El Mostafa Ketatni,[b] Francis Abraham,[a] and Olivier Mentré[a,*]

[a] *Laboratoire de Cristallochimie et Physicochimie du Solide, Universite des Sciences et Technologies de Lille, UMR CNRS 8012, ENSCL, B.P. 108, F-59652 Villeneuve d'Ascq Cedex, France*

[b] *Laboratoire d'Electrochimie et Chimie des Matériaux, Faculté des Sciences et Technique Cadi Ayyad, B.P. 523, Béni Mellal, Morocco*

Received 16 April 2003; received in revised form 1 July 2003; accepted 17 July 2003

Abstract

The crystal structure of the new $Bi_{\sim 3}Cd_{\sim 3.72}Co_{\sim 1.28}O_5(PO_4)_3$ has been refined from single crystal XRD data, $R_1 = 5.37\%$, space group *Abmm*, $a = 11.5322(28)$ Å, $b = 5.4760(13)$ Å, $c = 23.2446(56)$ Å, $Z = 4$. Compared to $Bi_{\sim 1.2}M_{\sim 1.2}O_{1.5}(PO_4)$ and $Bi_{\sim 6.2}Cu_{\sim 6.2}O_8(PO_4)_5$, this compound is an additional example of disordered Bi^{3+}/M^{2+} oxyphosphate and is well described from the arrangement of double $[Bi_4Cd_4O_6]^{8+}$ (= *D*) and triple $[Bi_2Cd_{3.44}Co_{0.56}O_4]^{6+}$ (= *T*) polycationic ribbons formed of edge-sharing $O(Bi,M)_4$ tetrahedra surrounded by PO_4 groups. According to the nomenclature defined in this work, the sequence is *TT*/*DtDt*, where *t* stands for the tunnels created by PO_4 between two subsequent double ribbons and occupied by Co^{2+}. The HREM study allows a clear visualization of the announced sequence by comparison with the refined crystal structure. The Bi^{3+}/M^{2+} statistic disorder at the edges of *T* and *D* entities is responsible for the PO_4 multi-configuration disorder around a central P atom. Infrared spectroscopy and neutron diffraction of similar compounds (without the highly absorbing Cadmium) even suggests the long range ordering loss for phosphates. Therefore, electron diffraction shows the existence of a modulation vector $q^* = 1/2a^* + (1/3 + \varepsilon)b^*$ which pictures cationic ordering in the (001) plane, at the crystallite scale. This ordering is largely lost at the single crystal scale. The existence of mixed Bi^{3+}/M^{2+} positions also enables a partial filling of the tunnels by Co^{2+} and yields a composition range checked by solid state reaction. The title compound can be prepared as a single phase and also the $M = Zn^{2+}$ term can be obtained in a biphasic mixture. For $M = Cu^{2+}$, a monoclinic distortion has been evidenced from XRD and HREM patterns but surprisingly, the orthorhombic ideal form can also be obtained in similar conditions.

Keywords: Bismuth phosphate; Polycation; Crystal structure; XRD; ED/HREM

1. Introduction

By analogy with the δ-Bi_2O_3 fluorite type [1–4] that can be described from clusters of edge-sharing OBi_4 and $\square Bi_4$ tetrahedra, it was recently observed that most of the Bi, *M* oxyphosphates, with *M* a divalent cation, can be structurally described from infinite ribbons-like polycations formed by edge sharing $O[Bi,M]_4$ tetrahedra [5]. The width of the ribbons vary ranging from $n = 1, 2, 3\ldots$ tetrahedra. For instance, $BiMPO_5$ ($M = Co^{2+}$, Ni^{2+}, Mn^{2+}) [6–9] contain isolated infinite $[OBiM]^{3+}$ chains, one tetrahedron wide. BiM_2PO_6 [10–18] contain $(O_2BiM_2)^{3+}$ ribbons, two tetrahedra wide. The ribbons are surrounded by PO_4 tetrahedra sometimes leading to the creation of tunnels between two consecutive ribbons. This original description is particularly well suited to a number of these compounds, rather than the conventional MO_x polyhedra linkage, (i) first because it enables to establish topological relationship between the number of materials of these chemical systems [5]. (ii) Because, for a number of recently evidenced materials, the *M*/Bi statistical disorder that characterizes part of the edges-of-ribbons sites avoids a clear visualization of the crystal structure. As a matter of fact it appears that even if the polycations endure mixed species at the edges of

*Corresponding author. Fax: +33-03-20-43-68-14.
E-mail address: mentre@ensc-lille.fr (O. Mentré).

0022-4596/$ - see front matter © 2003 Elsevier Inc. All rights reserved.
doi:10.1016/S0022-4596(03)00413-4

ribbons, it is responsible for a strong PO_4 disorder in the inter-ribbon space limiting their XRD characterization. For instance, the $Bi_{\sim 1.2}M_{\sim 1.2}O_{1.5}(PO_4)_1$ ($M = Mn^{2+}, Co^{2+}, Zn^{2+}$) cannot be described in terms of BiO_x–MO_y–PO_4 edifice but is satisfactorily described from disordered $(O_3Bi_{\sim 2.4}M_{\sim 1.6})^{+4.4}$ ribbons 3-tetrahedra wide. The peripheral sites are statistically occupied by 15% Bi and 85% M. The resulting polycations are surrounded by disordered PO_4 cations. The tunnels existing between two ribbons are partially occupied by M^{2+} ions [5]. Cations of different size can coexist in the same material. For instance, the recently reported $Bi_{\sim 6.2}Cu_{\sim 6.2}O_8(PO_4)_5$ contains both 2-tetrahedra wide $[Bi_{\sim 2.4}Cu_{\sim 3.6}O_4]^{6.4+}$ and 3-tetrahedra wide $[Bi_{\sim 5}Cu_{\sim 3}O_6]^{9+}$ ribbons alternating along a crystallographic axis and isolated by disordered phosphate groups [19]. The interstitial tunnels created between two different size ribbons are occupied by disordered Cu^{2+} cations. Most of the compounds adopt an orthorhombic unit cell with $a \sim 11.5$ Å, $b \sim 5.5$ Å and c depending on the ribbons sequence, e.g., we recently announced the values $c = 15.316(4)$ Å, $c = 38.57(2)$ Å and $c = 23.327(5)$ Å, for the major phase of the mixtures corresponding to the BiMCdPO$_6$ compositions with M = Ni, Cu and Zn, respectively [5]. For the latter, the corresponding crystal structure is original and is presented in this work. The prepared single crystals yield the approximate $Bi_{\sim 3}Cd_{\sim 3.72}Co_{\sim 1.28}O_5(PO_4)_3$ formula. It shows a crystal structure based on 2- and 3-tetrahedra wide ribbons new arrangement. Isomorphic materials were also prepared in the Bi_2O_3–CuO–CdO–P_2O_5 and Bi_2O_3–ZnO–CdO–P_2O_5 systems. In the disordered members of this family, PO_4 disorder clues are given by infrared microscopy and neutron diffraction. The use of complementary tools such as, electron diffraction microscopy and HREM images, enables a good correlation between these materials and related ones, help to strongly contrast polycations and phosphate groups. The observation of modulation at the microscopic scale is also discussed in this article.

2. Experimental

One should remind that the first allusion to the title compound existence was reported in Ref. [5] as the major phase of the BiCoCdPO$_6$ XRD pattern examination. To obtain single crystals of the title compound, BiCoCdPO$_6$ was fused in a gold crucible at 930° for 5 h and slowly cooled at 1°C/h to 800°. At this temperature the furnace was turned off to room temperature. Purple crystals corresponding to the new $Bi_{\sim 3}Cd_{\sim 3.72}Co_{\sim 1.28}O_5(PO_4)_3$ were extracted from the homogeneous melt. The different $Bi_wM_xCd_yP_z$ oxides (M = Co, Cu, Zn, Ni) reported in this work have been prepared from the stoichiometric mixtures of Bi_2O_3, CdO, MO and $(NH_4)_2HPO_4$. To avoid the problem of volatile species removal which implies a several heating-grinding steps reaction from 200°C to 800°C for phosphate synthesis, the reactants have been dissolved in nitric acid and homogenized by magnetic stirring. A small amount of citric acid was added in order to complex and disperse the cations in the solution. It was then heated at 150° up to total evaporation. The resulting powder was then dried, transferred in an alumina crucible and heated at 5°C/h to 800° for 48 h and quenched to room temperature. The purity of the samples were checked by the powder X-ray diffraction with a Siemens D-5000 diffractometer equipped with a graphite crystal diffracted-beam monochromator and Cu$K\alpha$ radiation.

FTIR spectra were recorded with a Perkin-Elmer spectrometer supplied with an attenuated total reflectance (ATR) accessory, with a press in order to get a very good optical contact between the crystal and the film. The samples were analyzed by means of diamond crystal prism. The crystal geometry was a 45° triangle with mirrored angle faces. ATR spectra are shown with an absorbance scale corresponding to $\log(R_{\text{reference}}/R_{\text{sample}})$, where R is the internal reflectance of the device. The spectra were recorded between 1100 and 750 cm^{-1} with 4 cm^{-1} spectral resolution. For each spectrum, 10 scans were co-added. As a reference air was simply taken.

Electron diffraction (ED) patterns and high-resolution images were obtained on a Jeol 200CX and a Jeol 400EX with a point resolution of 1.7 Å. In each case, the materials were crushed and dispersed on a holey carbon film deposited on a Cu grid. The computer simulated HREM images were calculated using JEMS program [20].

The experimental density measured using a Micrometritics Accupyc 1330Helium pycnometer yields $d_{\text{exp}} = 6.52$ g/cm^3 matching with the 6.65 g/cm^3 calculated value.

3. Single crystal X-ray analysis

3.1. Structure refinement

A purple single crystal was mounted on a glass fiber and exposed to X-rays. The diffraction intensities were measured on an AXS Bruker SMART CCD-1K diffractometer under the conditions given in Table 1 and extracted from the collected frames using the program SaintPlus 6.02 [21]. The orthorhombic lattice parameters $a = 11.5322(28)$, $b = 5.4760(13)$, $c = 23.2446(56)$ Å were refined from the complete data set. An absorption correction based on the faces indexation was performed using the program XPREP of the SHELXTL block [22]. Data were re-corrected

Table 1
Crystal data, measurement and structure refinement parameters for $Bi_3Cd_{3.72}Co_{1.28}O_5(PO_4)_3$

Crystal data	
Crystal symmetry	Orthorhombic
Space group	*Abmm*
Cell dimension (Å)	$a = 11.5322(28)$ Å
	$b = 5.4760(13)$ Å
	$c = 23.2446(56)$ Å
Volume (Å^3)	$V = 1467.9(6)$ (Å^3)
Z	4
Data collection	
Equipment	Bruker SMART CCD
λ (Mo$K\alpha$ (graphite monochromator)) (Å)	0.7107
Density calc.	6.859 g/cm^3
Color	Purple
Scan mode	ω
Θ max (deg)	63.11
Recording reciprocal space	$-16 \leqslant h \leqslant 16$, $-7 \leqslant k \leqslant 8$, $-33 \leqslant l \leqslant 31$,
Number of measured reflections	4320
Number of independent reflections	1379
μ (mm^{-1})(for $\lambda K\alpha = 0.7107$)	42.71
Limiting faces and distances (mm) from an arbitrary origin	$1\ \bar{1}\ \bar{4}$ 0.0150, $\bar{1}\ 1\ 4$ 0.0150, $\bar{5}\ \bar{1}\ \bar{2}$ 0.0410, $0\ 0\ 1$ 0.0160, $\bar{1}\ 1\ \bar{6}$ 0.0400, $2\ 1\ \bar{2}$ 0.0390
Refinement	
Number of refined parameters	113
Refinement method	Least square on F
$R_1(F)[I > 2\sigma I]/R_1(F)$ (all data)	0.0537/0.0651
$wR_2(F^2)[I > 2\sigma I]/wR_2(F^2)$ (all data)	0.1343
$w = 1/(\sigma^2(F_o^2) + (0.0700^*P)^2 + 0.00^*P)$ with $P = (\mathrm{Max}(F_o^2, 0) + 2^*F_c^2)/3$	
Goof	1.042
Max/Min $\Delta\rho$ (e^{-3})	0.52/0.01 e^{-3}

from the detector absorption using the program SADABS [23] with an μr value of 0. The systematic extinction conditions observed, $h\,k\,l : k + l = 2n$ and $0\,k\,l : k = 2n$ suggested two possible space groups: *Abm*2 or *Abmm*. The crystal structure refinement was performed in both but satisfactorily converged in the latter. The 2731 significant reflections ($I > 3\sigma(I)$) were merged in the *mmm* Laue group, leading to 564 unique reflections, $R_{int} = 6.83\%$.

Bi1, Bi2, Cd3 and Cd4, were first located in one 4(g) and three 8(m) special positions using the SHELXS Patterson option. The following part of the refinement was performed using the JANA 2000 program [24] and a least-squares matrix on F. The subsequent Fourier difference synthesis located O1, O2, O3, P1 and P2 yielding $R_1 = 12.8\%$. Intense peaks were then observed on the next Fourier difference map suggesting anisotropic displacement for the Bi and Cd atoms, $R_1 = 9.9\%$. At this stage of the refinement, a mixed Cd/Co occupancy on two adjacent positions was considered instead of Cd3 because of its low U_{iso} value. Co_a and Co_b two cobalt atoms were located on the subsequent Fourier difference calculation map. As detailed below, because of their particular role within the framework, their occupancies were refined, leading to $R_1 = 7.8\%$. The choice of JANA was more or less driven by the versatile use of rigid body option suiting well the disordered state of this series of materials. Effectively, at this stage the phosphates O^{2-} corners appeared at the next Fourier-difference synthesis and we know, by experience, the difficulty to locating/refining acceptable PO_4 considering the average superposition of a number of independent configurations centered at the same position. Around P1 four independent O positions forming two roughly regular tetrahedra ($P1O_4$ and its image by $m \perp b$) are located. Similarly, P2 is surrounded by two sets of O_4 groups roughly tetrahedral ($P2O_4$ and its image by $m \perp c$). Then, both PO_4 have been assigned to a perfect tetrahedral entity (T_d point symmetry, P–O = 1.54 Å). In a first stage, rotation angles by φ/a, χ/b, Ψ/c and displacement Δx, and Δz (for $P1O_4$), Δx for $P2O_4$ have been refined. In a second stage, the T_d symmetry of the group was broken by refining atomic coordinates for both molecular parts. The oxygen occupancies around phosphorus atoms have been fixed to $\frac{1}{2}$, in order to conserve the P/O ratio $= \frac{1}{4}$. Thus, the symmetry of the *Abmm* space group generates two equivalent PO_4 configurations around each phosphorus with equal occupancies. Fig. 1 shows the two configurations around P1 and P2. The refinement converged to $R_1 = 6\%$. It is noteworthy that for each group, oxygen displacement were restrained equal, leading to large values. Therefore, for reasons explained above, the perfect modelization of phosphate groups in this kind of structures looks utopic considering their medium range ordering. Attempts to consider independent atomic parameters did not lead to acceptable PO_4 edifices. In the last cycles of the refinement, anisotropic displacements were considered for every Bi, Cd, Co and for P2, secondary extinction was refined and a restriction on Co_a and Co_b was added to provide electroneutrality yielding final $R_1 = 0.0537$, $wR_2 = 0.1343$. The atomic coordinates with isotropic and anisotropic thermal parameters are listed in Tables 2 and 3. Table 4 provides selected bond distances and angles in $Bi_{\sim 3}Cd_{\sim 3.72}Co_{\sim 1.28}O_5(PO_4)_3$.

3.2. *Abmm* choice

The disappearing of the mirror perpendicular to the c-axis did not improve the refinement: *Abmm*, 19 atoms,

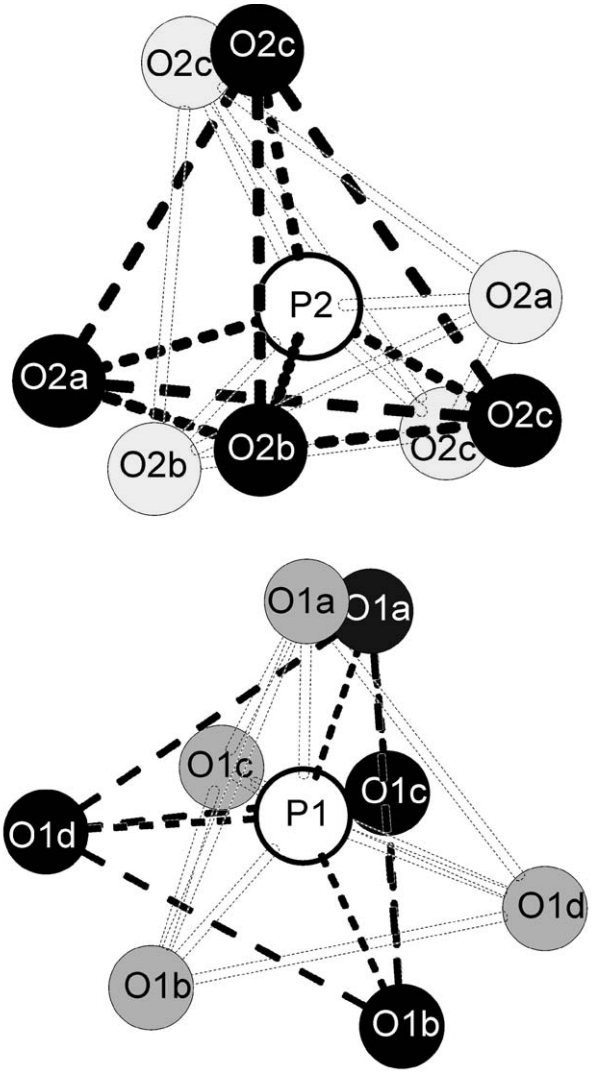

Fig. 1. The two refined PO_4 configurations around P1 and P2 showing the ideally modelled disorder.

58 refined parameters, $R_1 = 5.37\%$ versus *Abm*2, 39 atoms, 82 refined parameters, $R_1 = 5.20\%$. As a matter of fact, the symmetry lowering leads to the split of equivalent positions, e.g., the four atoms defining the polycationic ribbons (Bi1, Bi2, Cd3/Co3 and Cd4) transform into seven independent positions in *Abm*2, whereas split atoms do not significantly shift from their central position in *Abmm*. Furthermore, the refinement in *Abm*2 do not fix the Cd3/Co3 mixed occupancy problem. It was also expected that the several PO_4 configurations superposed on the same central P1 and P2 positions would split on independent sites of the *Abm*2 space group, but on the other hand the Fourier difference peaks observed around the three phosphorus positions (P1a, P1b and P2a in the *Abm*2 space group) are much more disordered and involve between 2 and 3 unregular PO_4 configurations for each.

4. Results and discussion

4.1. Ribbons concept

As already reported in analogue compounds, namely $Bi_{\sim 1.2}M_{\sim 1.2}O_{1.5}(PO_4)$ (M = Mn, Co, Zn) [5] and $Bi_{\sim 6.2}Cu_{\sim 6.2}O_8(PO_4)_5$ [19], the mixed occupancy over Co3/Cd3 positions and the statistical distribution of Co_a and Co_b on positions superimposed along the b-axis are responsible for the disorder of several PO_4 configurations around the same central P1 and P2 crystallographic positions. It is such that we developed, a new descriptive concept based on the $O(Bi,M)_4$ tetrahedra association in polycationic ribbons of variable width. This model allows us to bypass the difficult problem of Bi^{3+} and M^{2+} accurate anionic coordination in so-disordered systems. For instance, the recently published $Bi_2MnO_4(PO_4)_2$ [25] that shows comparable disorder phenomena, may be better described in term of helix-like arrangement of triple polycationic ribbons related by a four-fold axis and isolated by PO_4 groups. Furthermore, evidence of topological relationship between a number of Bi–X–O (X being a tetrahedral cation) was pointed out. In fact, it appears that the oxygen atoms that do not belong to the XO_4 groups are at the center of the previously cited $O(Bi, M)_4$ tetrahedra. They share edges to form infinite cationic ribbons surrounded by XO_4 tetrahedra. The formed framework is dependent on their width, e.g., single (= S) chains in $BiMPO_5$ (X = Co, Ni) [6–9], 2-tetrahedra wide ribbons (= D) in BiM_2XO_6 [10–18], 3-tetrahedra wide ribbons (= T) in $Bi_{\sim 1.2}M_{\sim 1.2}O_{1.5}(PO_4)$ [5], and both T and D in $Bi_{\sim 6.2}Cu_{\sim 6.2}O_8(PO_4)_5$ [19]. In some cases, transition metals directly bonded by PO_4 corners forming tunnels (= t) are located between two subsequent polycations, e.g., Co_a and Co_b in the title compound. A nomenclature using the $T-D-t$ sequence along c, centered at $x = 0$, and the $T-D-t$ sequence centered at $x = \frac{1}{2}$, separated by/is useful. So $BiM_2O_2(PO_4)$ compounds adopts a D/D sequence, Fig 2a, $Bi_{\sim 1.2}M_{\sim 1.2}O_{1.5}(PO_4)$ adopts a Tt/Tt sequence, Fig. 2b. $Bi_{\sim 6.2}Cu_{\sim 6.2}O_8(PO_4)_5$ adopts a $DtTTt/TtDtT$ sequence, Fig. 2c. From our experience of this family several empirical rules have been deduced.

(a) The n-tetrahedra wide polycation can be formulated $[M_4Bi_{2n-2}O_{2n}]^{x+}$ where M stands for the edges of ribbons positions (possible Bi^{3+}/M^{2+} mixed nature) and Bi for the ribbons core of ribbons (solely Bi^{3+}).
(b) As explicitly suggested by the above ribbon formula, the ribbons core are solely occupied by Bi^{3+} cations while peripheral M positions can host a Bi^{3+}/M^{2+} mixed occupancy yielding the x^+ charge.
(c) Because of the ribbons organization, most of these materials crystallize in an orthorhombic unit cell

Table 2
Atomic positions and isotropic/equivalent displacement for $Bi_3Cd_{3.72}Co_{1.28}O_5(PO_4)_3$

Atom	Site	Occupancy	x	y	z	U or U_{eq}
Bi1	4*g*		0.39879(17)	0.00000	0.25000	0.027(7)
Bi2	8*m*		0.10488(13)	0.50000	0.05863(9)	0.033(5)
Cd3	8*m*	0.86(2)	0.6042(11)	0.00000	0.3567(3)	0.047(3)
Co3	8*m*	0.14	0.593(10)	0.00000	0.370(3)	0.010(4)
Cd4	8*m*		−0.0934(2)	0.50000	0.17155(12)	0.028(8)
O1	4*a*		0.00000	0.75000	0.00000	0.022(7)
O2	8*j*		0.50000	0.25000	0.3091(10)	0.036(5)
O3	8*j*		0.00000	0.25000	0.1161(9)	0.034(6)
Co_a	4*b*	0.37(9)	0.50000	0.25000	0.50000	0.060(2)
Co_b	8*i*	0.31(4)	0.50000	−0.059(10)	0.50000	0.110(2)
P1	8*m*		0.6939(12)	0.50007(8)	0.4176(6)	0.055(13)
O1a	16*o*	0.5	0.7987(12)	0.53560(8)	0.4571(6)	0.109(13)
O1b	16*o*	0.5	0.5878(12)	0.63990(8)	0.4412(6)	0.109(13)
O1c	16*o*	0.5	0.7240(12)	0.59270(8)	0.3568(6)	0.109(13)
O1d	16*o*	0.5	0.6654(12)	0.22150(8)	0.4155(6)	0.109(8)
P2	4*g*		−0.1803(13)	0.00000	0.25000	0.048(6)
O2a	8*m*	0.5	−0.204(6)	0.00000	0.323(4)	0.125(15)
O2b	8*m*	0.5	−0.292(5)	0.00000	0.233(3)	0.125(15)
O2c	16*o*	0.5	−0.133(3)	0.251(7)	0.239(3)	0.125(15)

Table 3
Anisotropic temperature factor for components (in $Å^2$) for $Bi_3Cd_{3.72}Co_{1.28}O_5(PO_4)_3$

Atom	U_{11}	U_{22}	U_{33}	U_{12}	U_{13}	U_{23}
Bi1	0.0158(9)	0.0187(11)	0.0474(15)	0.00000	0.00000	0.00000
Bi2	0.0289(8)	0.0232(7)	0.0469(9)	0.00000	−0.0122(9)	0.00000
Cd3	0.054(5)	0.025(2)	0.062(6)	0.00000	−0.031(5)	0.00000
Cd4	0.0327(14)	0.0170(11)	0.0350(15)	0.00000	0.0034(13)	0.00000
P2	0.025(7)	0.039(9)	0.080(12)	0.00000	0.00000	0.00000
Co_a	0.047(16)	0.12(7)	0.012(12)	0.00000	0.00000	0.00000
Co_b	0.15(2)	0.08(7)	0.103(19)	0.00000	−0.10(2)	0.00000

Table 4
Selected *M*–O bonds lenghts (Å) for $Bi_3Cd_{3.72}Co_{1.28}O_5(PO_4)_3$

Bi, Cd, Co (ribbons) distances			
Bi1–O2 × 4	2.263(14)	Bi2–O1 × 2	2.279(14)
Cd3–O2 × 2	2.132(14)	Bi2–O3 × 2	2.262(12)
Cd4–O3 × 2	2.167(12)	Co3–O2 × 2	2.24(7)
PO_4 distances			
P1–O1a	1.529(15)	P2–O2a × 2	1.73(9)
P1–O1b	1.546(13)	P2–O2b	1.35(6)
P1–O1c	1.540(14)	P2–O2c	1.50(4)
P1–O1d	1.565(3)		
		O2a–P2–O2c	103 (3)
O1a–P1–O1b	110.32(73)	O2a–P2–O2c	103 (3)
O1c–P1–O1b	109.76(72)	O2a–P2–O2b	98 (4)
O1d–P1–O1b	109.30(72)	O2c–P2–O2b	107 (2)
O1a–P1–O1d	108.20(72)	O2c–P2–O2b	107 (2)
O1d–P1–O1c	110.04(72)	O2a–P2–O2b	98 (4)
O1c–P1–O1a	109.20(72)		
Ideal Co (tunnels) distances			
Co_a–O1b × 4	2.730(7)	Co_b–O1b × 2	2.020(31)
Co_a–O1d × 4	2.742(11)	Co_b–O1b × 2	2.369(39)
Co_a–O1d × 4	1.805(11)		

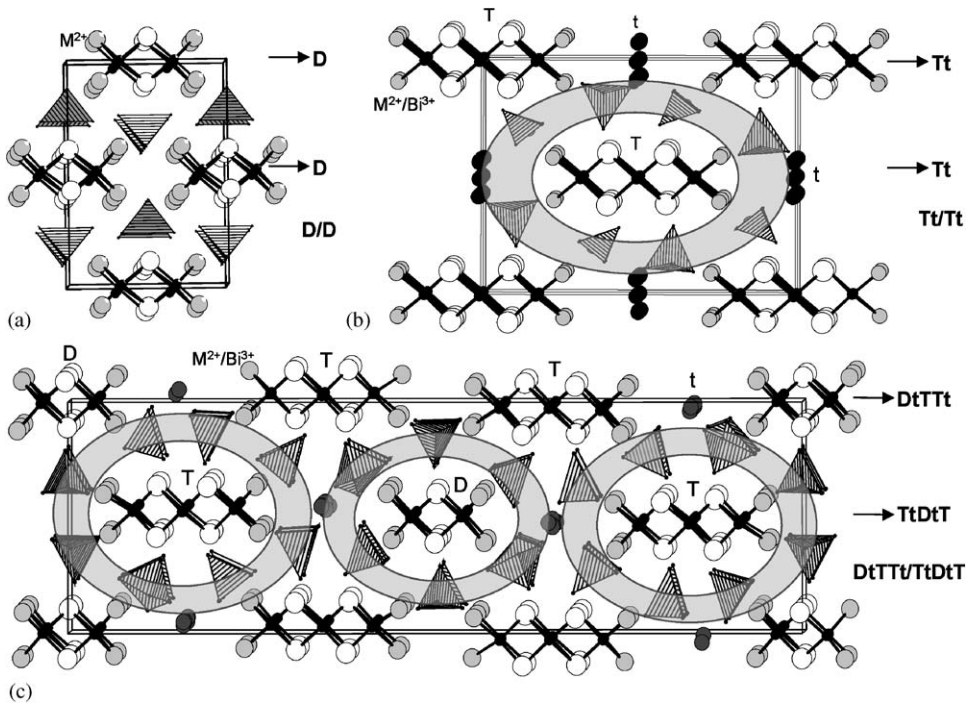

Fig. 2. Projection along (010) of the structures of other ribbons-possessing compounds, showing the T, D, t nomenclature: (a) BiM_2PO_6, (b) $Bi_{\sim 1.2}M_{\sim 1.2}(PO_4)O_{1.5}$, (c) $Bi_{\sim 6.2}Cu_{\sim 6.2}(PO_4)_5O_8$. The gray crown pictures the disordered space existing because of the mixed nature of some edge of ribbons sites (gray atoms).

with two common parameters. The first one (conventionally the a-axis), ~ 11.5 Å, corresponds to twice the distance between two parallel ribbons. The second, ~ 5.5 Å (conventionally the b-axis) is ruled by the ribbon structure and corresponds to the height of two edge-shared $O(Bi,M)_4$ tetrahedra along the infinite axis.

(d) Theoretically, the ribbons size is unlimited, ranging from single chains in $BiMO(PO_4)$ [1–4] to infinite $[Bi_2O_2]^{2+}$ planes in Aurivillius isotype compounds such as $Bi_4V_2O_{11}$ [26,27].

(e) Ribbons of different size can coexist in the same material, e.g., T and D with different arrangement in $Bi_{\sim 6.2}Cu_{\sim 6.2}O_8(PO_4)_5$ and in the title compound.

(f) Considering the crystal structure, it appears rather instructive to formulate the compounds in order to evidence the different polycations, surrounding phosphates and interstitial cations. Thus, $Bi_{\sim 6.2}Cu_{\sim 6.2}O_8(PO_4)_5$ is better formulated $[Bi_{2.4}Cu_{3.6}O_4]_1[Bi_5Cu_3O_6]_2Cu_{2.8}(PO_4)_{10}$ with the $DtTTt/TtDtT$ sequence. This model is particularly well-adapted to HREM photographs that highlight the PO_4/ribbons contrast.

4.2. Structure description

According to that formalism, O1 and O3 form 3-tetrahedra wide cations with $O1Bi2_4$ central tetrahedron sharing edges with two $O3Bi2_2Cd4_2$ tetrahedra. It yields the formation of $[Bi_4Cd_4O_6]^{8+}$ triple ribbons (= T) with central Bi-only and peripheral Cd-only positions, from the single crystal XRD analysis, Fig. 3a. O2 are at the center of $Bi2_2Cd/Co3_2$ tetrahedra that share edges two by two along the c-axis to form $[Bi_2Cd_{3.44}Co_{0.56}O_4]^{6+}$ double ribbons with mixed Cd/Co (86%–14%) extremities(= D), Fig. 3b. Inside the ribbons, M–O bonds range from 2.13(2) to 2.279(14) (Fig. 3).

The Co_a and Co_b cations occupy tunnels (= t) parallel to the b axis formed by the $P1O_4$ groups located between two consecutive $[Bi_2Cd_{3.44}Co_{0.56}O_4]^{6+}$ double ribbons along c. The compound formula is $Bi_3Cd_{3.72}Co_{1.28}O_5(PO_4)_3$, $Z = 4$ that can be developed $[Bi_4Cd_4O_6]_2[Bi_2Cd_{3.44}Co_{0.56}O_4]_2Co_4(PO_4)_{12}$ taking account of ribbons and tunnels. The sequence of the title compound is $TT/DtDt$ as evidenced in Fig. 4.

4.3. Tunnels occupancy

Considering two tunnels/unit cell, along $\langle \frac{1}{2}, z, 0 \rangle$ and $\langle \frac{1}{2}, z, \frac{1}{2} \rangle$, and a minimal Co–Co distance of 2.8 Å within tunnels, they can be considered filled for about 4 Co_a–Co_b/unit cell which is verified at the end of the crystal structure refinement. It is noteworthy that independent refinement of Co_a and Co_b occupancies without any restraint leads to values very close to the presented ones. Therefore, to guaranty electroneutrality a restraint relating these parameters was added. From Fig. 5a

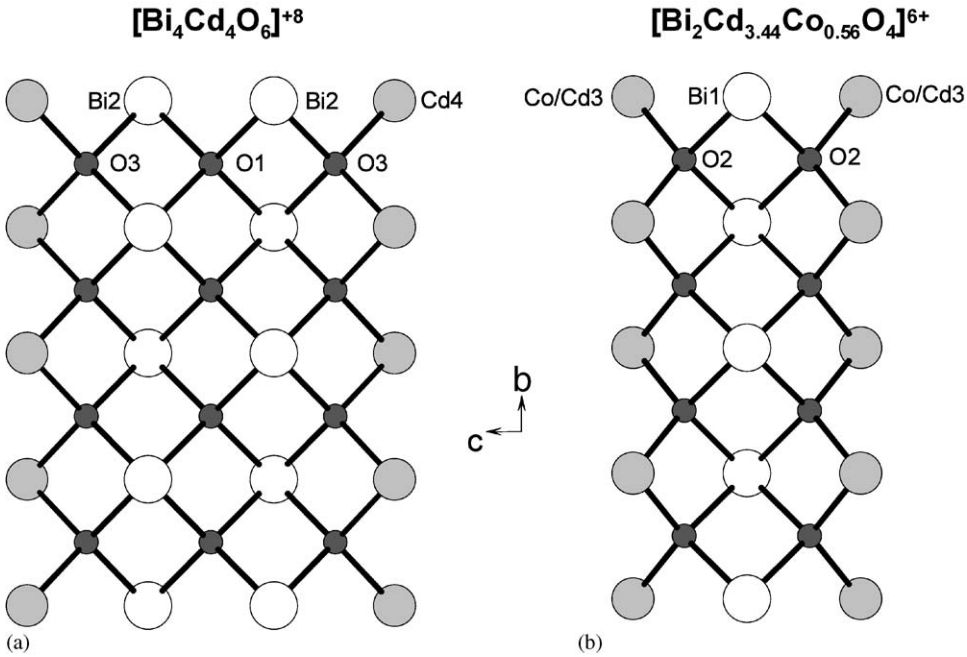

Fig. 3. The $[Bi_4Cd_4O_6]^{+8}$ ribbons (3-tetrahedra wide = T) and the $[Bi_2Cd_{3.44}Co_{0.56}O_4]^{+6}$ polycations (2-tetrahedra wide = D) with the label scheme. Each oxygen is tetrahedrally coordinated by Bi, Cd and Co.

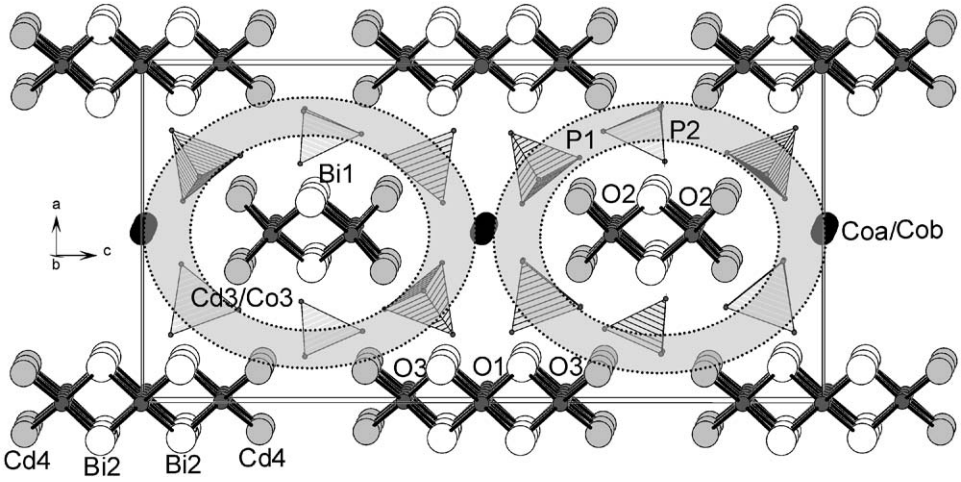

Fig. 4. Projection along the (010) direction of $Bi_3Cd_{3.72}Co_{1.28}O_5(PO_4)_3$ structure: the gray circles show the disorder zones.

which presents all the possible Co_a and Co_b positions surrounded by all the possible $P1O_4$ configurations, we tried to establish the real tunnels occupancy and cobalt environments. Thus, tunnels being fully filled, a segregation of $\cdots$–Co_a–Co_a–Co_a–$\cdots$ and $\cdots$–Co_b–Co_b–Co_b–$\cdots$ long chains is expected leading to reasonable Co–Co distance of 2.738(77). A great number of –Co_a–Co_b– interfaces within the same tunnel (Co_a–Co_b = 3.78(5) Å) would lead to a significant deviation of the Co_a and Co_b occupancies towards partially empty tunnels. So, as shown on the Fig. 5b, inside Co_a segments, two Co_aO_x kinds of polyhedra would alternate along b, octa-coordinated Co_aO_8 with Co–O ranging from 2.730(7) to 2.742(11) Å, and tetra-coordinated Co_aO_4 with Co–O distances of 1.805(11) Å in a distorted square planar configuration. In the same manner, Co_b segments would be formed of edge-sharing regular Co_bO_4 tetrahedra with Co–O distances include the 2.020(31)–2.369(39) Å range (Fig. 5c). This model enables to propose likely Co–O coordination with one unique PO_4 configuration per P site. One should also consider that modifications of these ideal configurations are probable because of imprecisions on phosphate oxygen refinement parameters.

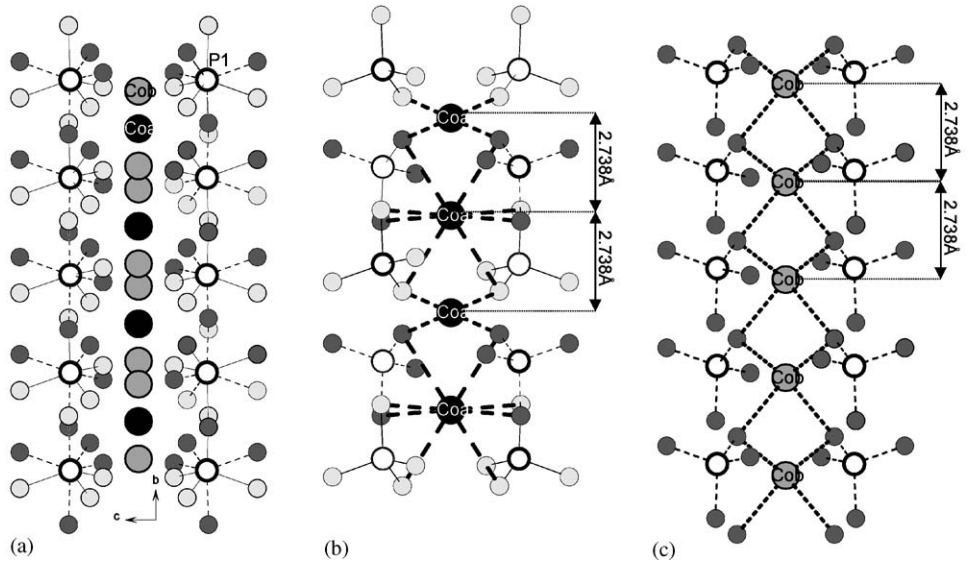

Fig. 5. The tunnels occupancy along the b axis: (a) All the available interstitial Co_a/Co_b sites (Co_a in black circles and Co_b in gray circles) surrounded by all the possible $P1O_4$. According to the complete occupancy of the tunnels, from distances considerations two possible arrangements are pointed out: (b) $–Co_a–Co_a–Co_a–$ segments which alternate octahedral and distorted square planar Co_a cations. (c) Tetrahedral $–Co_b–Co_b–Co_b–$ segments.

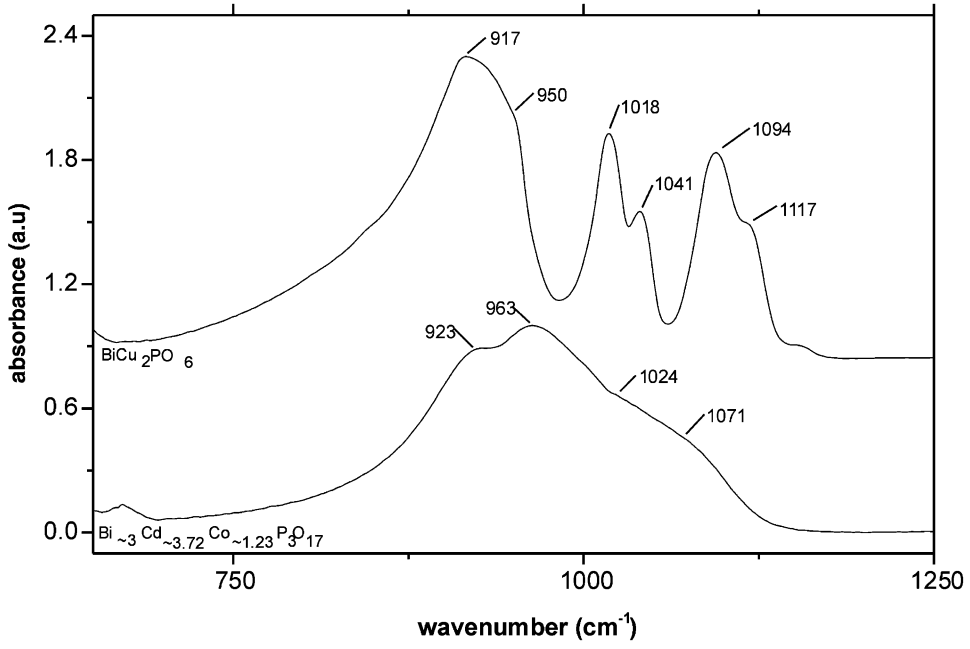

Fig. 6. Infrared spectra of the ordered $BiCu_2PO_6$ (ordered compound) and the disordered $Bi_3Cd_{3.72}Co_{1.28}O_5(PO_4)_3$.

4.4. PO_4 disorder

The PO_4 disordering over a number of configurations surrounding one central phosphorus atom is a direct consequence of the ability of the ribbons to host mixed Bi^{3+}/M^{2+} cations at their edges. It means that, depending on the $Bi^{3+}/Co^{2+}/Cd^{2+}$ nature, the surrounding oxygen environment brought by PO_4 corners will be drastically modified. This is the main reason for the systematical PO_4 location difficulties by XRD analysis. Fig. 6 shows infrared spectra of the well-ordered $BiCu_2PO_6$ [17] (D/D sequence) with Cu^{2+}-only at the edges of the double ribbons and one kind of well located PO_4. It shows a number of well-defined P–O bands between 750 and 1100 cm^{-1}. On the contrary, the title compound shows the overlapping of broad peaks picturing the statistic disordering of PO_4 multi-configurations. Furthermore, neutrons diffraction experiments, very sensitive to the oxygen weight, performed on similarly disordered materials—but not on the title

Table 5
Summary of the different syntheses attempted to prepare the title compound and isomorphic materials. The tunnel occupancy is reported in case of nearly pure sample

	Purity	Refined parameters	M/Cd tunnels occupancy
$M=Co^{2+}/Cd^{2+}$			
$Bi_3Cd_{3.72}Co_{1.28}(PO_4)_3O_5$	Pure	$a = 11.5850(30)$ Å, $b = 5.4909(15)$ Å, $c = 23.3187(78)$ Å	100%
$Bi_{3.4}Cd_{3.4}Co_1(PO_4)_3O_5$	Pure	$a = 11.5764(57)$ Å $b = 5.4888(20)$ Å $c = 23.3191(1\,0\,5)$ Å	80%
$Bi_3Cd_3Co_3(PO_4)_3O_6$	Impurity: Co_3O_4	$a = 11.556(3)$ Å $b = 5.485(1)$ Å $c = 23.327(5)$ Å	
$M=Zn^{2+}/Cd^{2+}$			
$Bi_3Cd_3Zn_3(PO_4)_3O_6$	Impurity: ZnO	$a = 11.590(5)$ Å $b = 5.489(2)$ Å $c = 23.250(5)$ Å	
$Bi_3Cd_{3.72}Zn_{1.28}(PO_4)_3O_5$	Not pure ($c \sim 15$ Å)		
$M=Cu^{2+}/Cd^{2+}$			
$Bi_3Cd_{3.72}Cu_{1.28}(PO_4)_3O_5$	Pure	$a = 11.6383(1\,1\,7)$ Å $b = 5.4505(44)$ Å $c = 23.4725(1\,9\,0)$ Å	100%
$Bi_3Cd_{3.6}Cu_{1.2}(PO_4)_3O_{4.8}$	Pure	$a = 11.6329(34)$ Å $b = 5.4527(16)$ Å $c = 23.4546(74)$ Å	100%
$Bi_3Cd_{3.6}Cu_{1.2}(PO_4)_3O_{4.8}$	Weak impurity lines	$a = 11.5988(42)$ Å $b = 5.4474(22)$ Å $c = 23.3540(90)$ Å $\beta = 90.2535(3\,0\,9)^\circ$	80%
$Bi_{3.3}Cd_{3.3}Cu_{1.06}(PO_4)_3O_{4.8}$	Weak impurity lines	$a = 11.6499(70)$ Å $b = 5.4581(76)$ Å $c = 23.2627(1\,3\,3)$ Å	66%
$Bi_{3.26}Cd_{33.6}Cu_{1.08}(PO_4)_3O_{4.85}$	Not pure: ($c \sim 38$ presence)		
$M=Cd^{2+}$			
$Bi_{3.872}Cd_{3.698}(PO_4)_3O_5$	Pure	$a = 11.6485(21)$ Å[a] $b = 5.5452(10)$ Å[a] $c = 23.4369(42)$ Å[a]	57%
$Bi_{3.7}Cd_{3.7}(PO_4)_3O_{4.76}$	Not pure: ($c \sim 38$ presence)		

[a] Crystal parameters.

compound because of the highly absorbent Cd presence—unambiguously shows a very high background as compared to $BiCu_2PO_6$ neutron pattern while their XRD patterns both indicate sign of a comparable good crystallinity. This observation strongly suggests that PO_4 long-range ordering is largely lost in these materials while the ribbons framework is conserved, so leading to diffuse scattering of oxygen ions.

4.5. Composition

It is rather hazardous to distinguish the structure type dependence on the transition metal nature since, from our experience, the $c \sim 8$ Å (D/D type), the $c \sim 15$ Å (Tt/Tt-type $Bi_{\sim 1.2}M_{\sim 1.2}O_{1.5}(PO_4)$ [5]), the $c \sim 23$ Å ($TT/DtDt$ type, e.g., this study) or the $c \sim 38$ Å ($TtTTt/TtDtT$-type $Bi_{\sim 6.2}M_{\sim 6.2}O_8(PO_4)_5$ [19]) can indifferently be obtained with $M^{2+} = Co^{2+}$, Zn^{2+}, Cu^{2+}, Cd^{2+}, Mn^{2+} … but rarely as single phase. In a general way, attempts to prepare single phase with a $3d$ transition metal-only for M^{2+} leads to predominant BiM_2XO_6 in the reaction product, while M^{2+}/Cd^{2+} mixture appears very efficient to control the final product. Furthermore, during our synthesis, it is not rare that attempt to prepare one structural type leads to another one or a mixture of several types, because of: (a) the relative closeness of these phases in the P_2O_5–Bi_2O_3–MO diagram. (b) The influence of the synthesis conditions, so far not ruled out. (c) The mixed Bi^{3+}/M^{2+} nature of edges of ribbons. (d) The possible partial occupancy of tunnels created between ribbons. For example, according to the M–M minimal distance of $\sim b/2$ criterion, e.g., 100% in the title compound, 80% in $[Bi_{4.8}M_{3.2}O_6]_1M_{1.6}(PO_4)_4$ (M = Co, Zn, Mn) and 70%

in $[Bi_{2.4}Cu_{3.6}O_4]_1[Bi_5Cu_3O_6]_2Cu_{2.8}(PO_4)_{10}$. At least we can announce that Cd^{2+} plays a key role since it preferentially occupies edges of ribbons with Bi^{3+}, so stabilizing long sequence of ribbons along c while the $3d$ transition metals have a tendency to host tunnels. Therefore, Cd^{2+} can also occupy the tunnel since materials isomorphic with the title compound have been prepared without other transition metal.

Table 5 reports several prepared compositions, according to the technique described in the experimental section. The purity determined from XRD patterns examination as well as the refined lattice parameters is noted. When the sample appears almost pure, the tunnel occupancy can be deduced, considering full occupancy on ribbons positions (core and edges). It is clear that $M^{2+} = Co^{2+}/Cd^{2+}$, Zn^{2+}/Cd^{2+}, Cu^{2+}/Cd^{2+} and Cd^{2+} only can lead to $c \sim 23$ materials. Therefore, it is noteworthy that in the Zn^{2+}/Cd^{2+} case, a compound possessing the $TT/DtDt$ sequence was obtained only for a Bi/Cd = 1, as it was mentioned in a previous paper [5].

For the $Bi_3Cd_{3.6}Cu_{1.2}(PO_4)_3O_{4.8}$ composition, a monoclinic distortion has been observed with lattice parameters $a = 11.599(4)$, $b = 5.447(2)$, $c = 23.354(9)$ Å and $\beta = 90.25(3)^\circ$. A zoom of split reflections $(10\bar{2})-(102)$ and $(21\bar{5})-(215)$ is shown in the insert of the Fig. 7, in comparison to the $Bi_3Cd_{3.72}Cu_{1.28}(PO_4)_3O_5$ XRD pattern fully indexed in the orthorhombic unit cell. As detailed below, this distortion was also evidenced on HREM images. We did not succeed in re-preparing monoclinic $Bi_3Cd_{3.6}Cu_{1.2}(PO_4)_3O_{4.8}$. Except the first time, our attempts failed leading to the orthorhombic lattice parameters: $a = 11.633(3)$, $b = 5.452(1)$, $c = 23.454(7)$ Å. A possible orthorhombic to monoclinic transition versus temperature is currently under investigation.

4.6. ED and HREM study

As shown in Fig. 8, examination of electron diffraction patterns of $Bi_3Cd_{3.72}Co_{1.28}O_5(PO_4)_3$ leads to the partial extinction symbol Ab- - (- means no glide plane) by comparison between the shift and difference of periodicity of the zero order Laue (ZOLZ) and first order Laue zone (FOLZ), according to the Morniroli's table [28]. This validates the crystal structure refined in

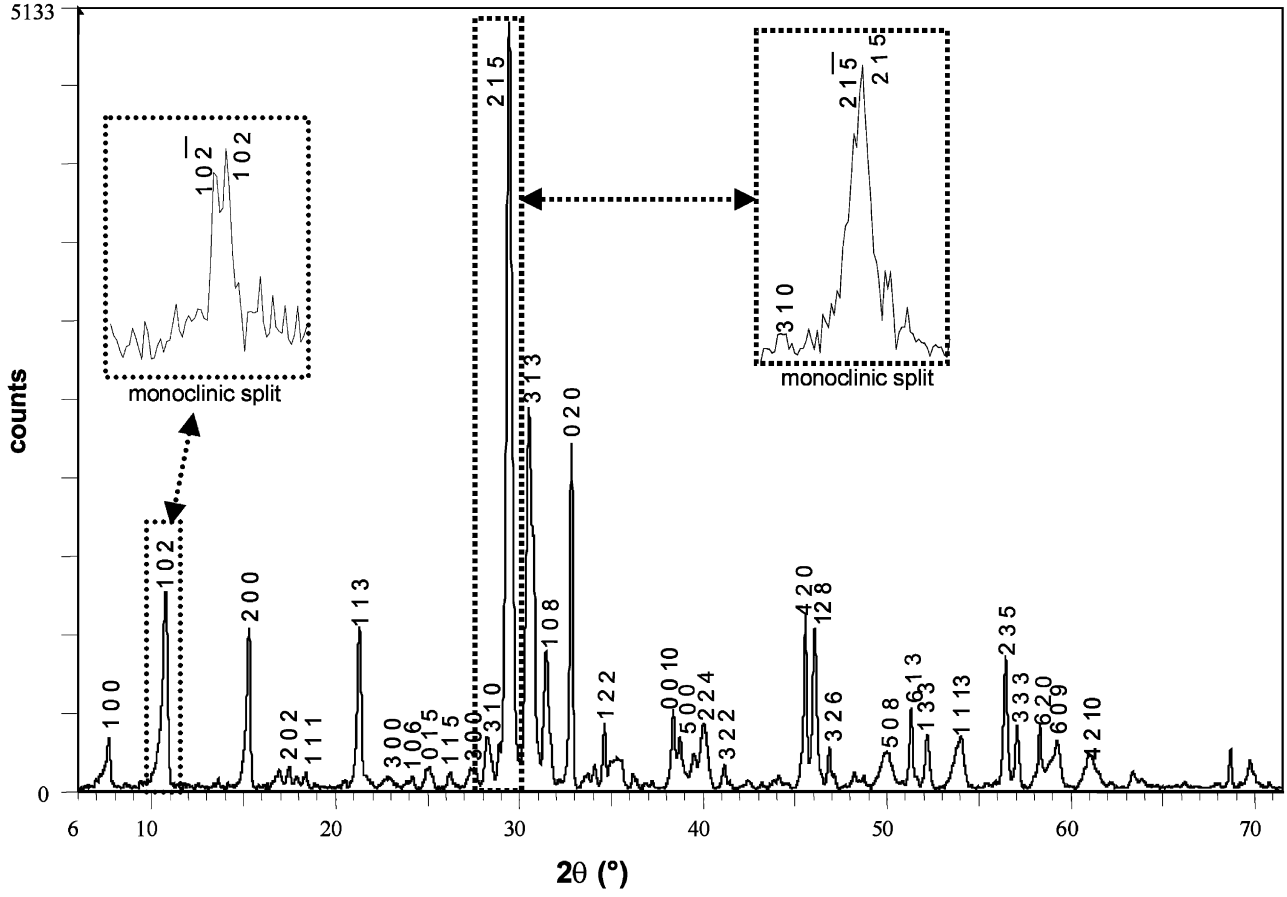

Fig. 7. Indexed XRD pattern for the orthorhombic $Bi_3Cd_{3.72}Co_{1.28}P_3O_{17}$. The inserts show the monoclinic split sometimes observed for the $Bi_3Cd_{3.6}Cu_{1.2}P_3O_{16.8}$ compound.

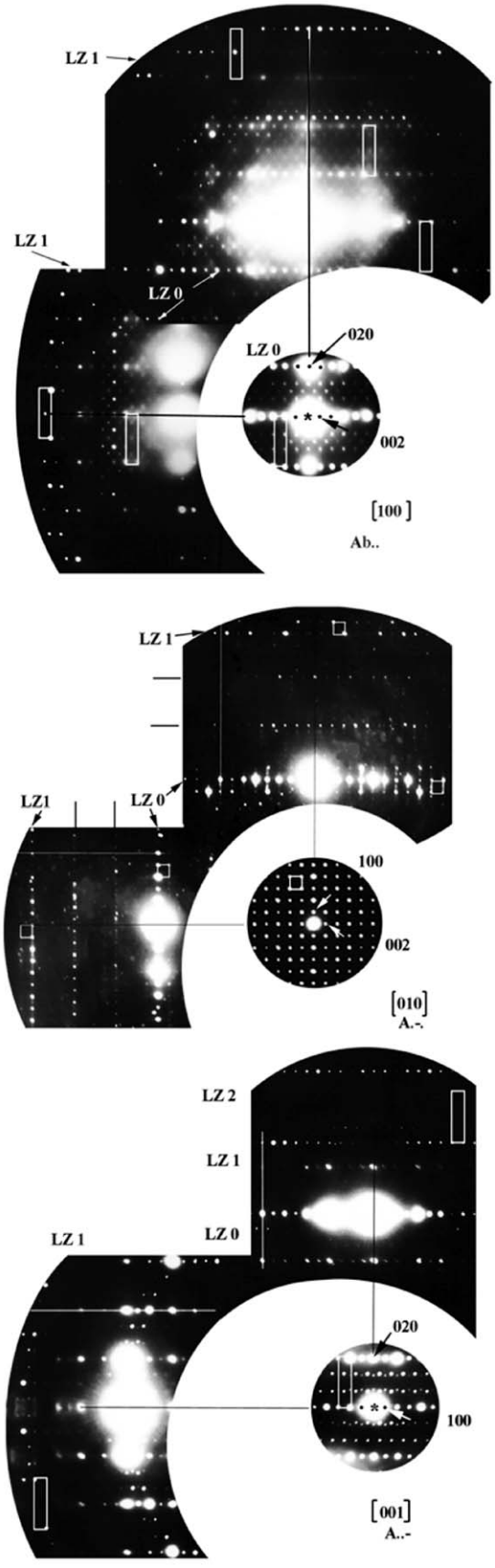

the Abmm space group, in good agreement with the indexation of intense spots in the basic cell. Supplementary weaker spots are evidenced and will be studied in a further work.

The [010] high-resolution (HR) images are informative since they reveal the width and $D-T-t$ sequence as shown in Fig. 9. This latter is constituted of seven parts a–g: Fig. 9a and b show a moderate enlargement of the experimental image and a magnification of the image, respectively, pointing out the conservation of a regular lattice with no defect such as twin or intergrowth. Fig. 9c is the image calculated on the basis of the structure refinement results, for a defocus of −200 Å and a thickness of 27 Å (conditions leading to a good accordance between experimental and simulated images). It allows to establish the direct relation between the structure projection and the observed contrast. It

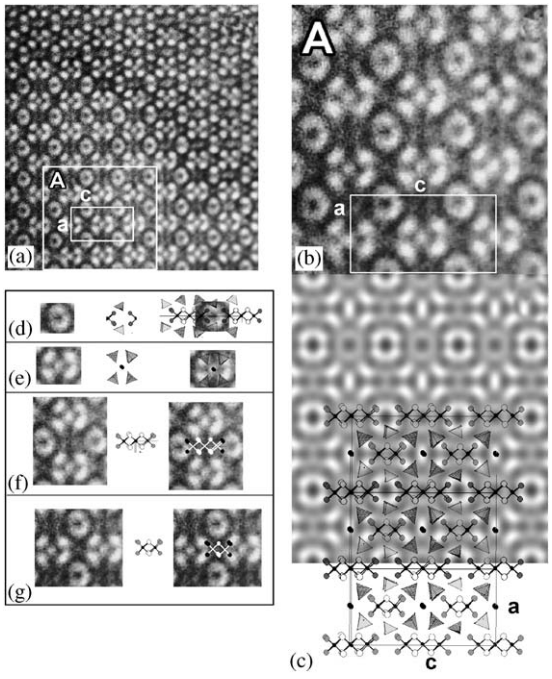

Fig. 9. $Bi_3Cd_{3.72}Co_{1.28}O_5(PO_4)_3$: [010] high resolution image revealing the width and sequence of the double and triple chains. (a) Moderate enlargement of experimental image (b) magnification of the zone A of (a). (c) Simulated image for a defocus of −200 Å and a thickness of 27 Å allowing a direct relationship between the structure projection and the observed contrast. (d–g) Cut of the experimental contrast described as a grid-like distribution of (d) white circle and (e) white cross. (d) White circles show triple chains edge and PO_4 groups. (e) White cross represents the four PO_4 groups forming the tunnel between two double ribbons. (f) Black zones between circles show the central part of the double chain (g) black contrast between two crosses show the double ribbon.

Fig. 8. $Bi_3Cd_{3.72}Co_{1.28}O_5(PO_4)_3$: (a) [100] (b) [010] (c) [001] zone axis patterns. The comparison between the shift and difference of periodicity of the zero order Laue zone and first order Laue zone leads to the partial extinction symbol Ab - - (- means no glide plane).

can be described as a grid–like distribution of white circle and white cross with each cross surrounded by four circles. From image simulation we can assign the various groups of the crystal structure to the apparent contrast as follows:

(a) the white circles are composed of T edges as well as surrounding $P2O_4$ groups, Fig. 9d;
(b) the white cross represents the four $P1O_4$ groups forming the tunnels between two subsequent D ribbons, Fig. 9e.
(c) the central white dot inside the cross is the Co_a and Co_b tunnels hosts.

Black zones between two circles along c show the central part of the T ribbons, Fig. 9f and e the black zones between two crosses show the D ribbons, Fig. 9g. Same contrast has been observed from the HREM study of the isomorphic $Bi_3Cd_3ZnO_5(PO_4)_3$. On the opposite, perturbation has been observed on crystals of $Bi_3Cd_{3.6}Cu_{1.2}(PO_4)_3O_5$, Fig. 10a. On these crystals diffuse streaks appear along c^* on the electron diffraction patterns. In the HREM patterns, the perturbation is easily observable in the thick part of the sample by modification of the periodicity along c (black arrows in Fig. 10a). Fig. 10b and c correspond to images compressed along b at different scales in order to exaggerate the undulation of the columns along c. It appears that the perturbation is due to a monoclinic distortion of the unit cell (Fig. 10c), as described in the last section of this work. This distortion yields a β angle close to 90° which frequently leads to $abc/\bar{a}bc$ twinned domains emulating the orthorhombic symmetry.

4.7. Additional phenomena

As we have mentioned before extra spots appear on the [001] and [100] EDP (Fig. 11). One can notice that the modulation phenomenon are the same for $M^{2+} = Co^{2+}$, Zn^{2+} and Cu^{2+} compounds.

[001] EDP (Fig. 11a): The pattern is indexed with a modulation vector $q^* = 1/2a^* + (1/3 + \varepsilon)b^*$. In the schematic representation of the pattern black points correspond to the basic spots, black crosses to the extinct basic spots, gray points to the modulation spots and gray crosses to the extinct modulation spots. This vector explains the difference of intensity between modulation spots (1st order is much intense than second order). Thus complex extinction sets are pointed out since $h\,1\,0\,\bar{1}$ and $h\,0\,0\,2$ spots are observed while $h\,1\,0\,\bar{2}$ and $h\,0\,0\,1$ are extinct. Since q lies in the (a, b) plane, it

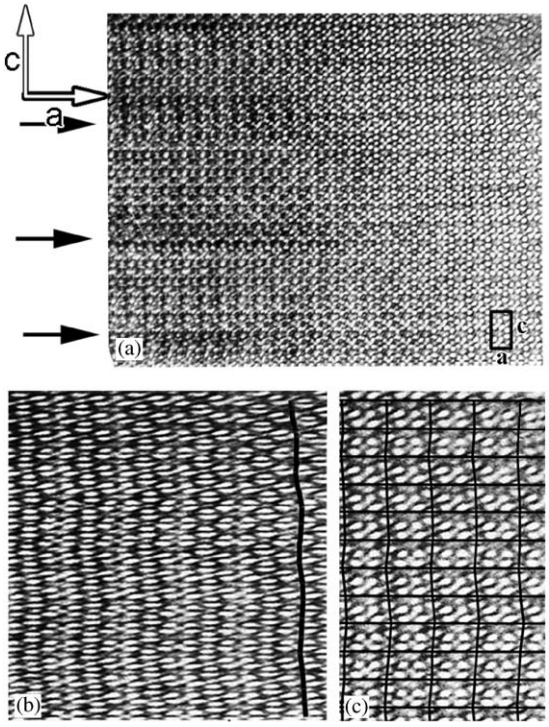

Fig. 10. $Bi_3Cd_{3.6}Cu_{1.2}O_5(PO_4)_3$: [010] high resolution image revealing distortion (a) easily observed in the thick part of the sample (black arrows) and evidenced in the thin part by artificial compressing of the cell along b in order to exaggerate the undulation (b) big and (c) moderate compression.

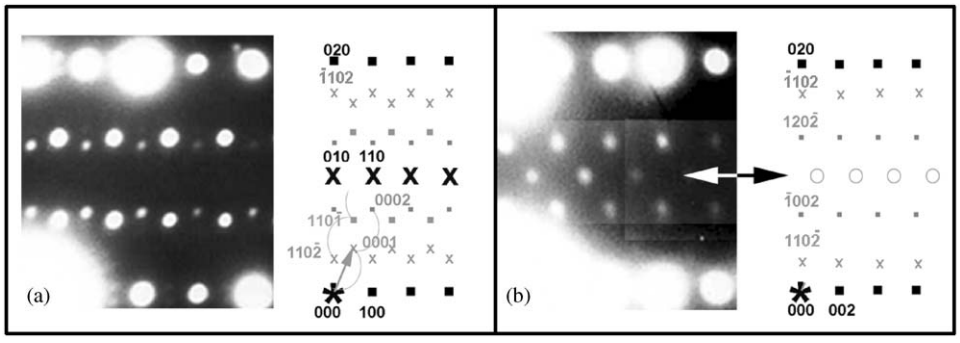

Fig. 11. $Bi_3Cd_{3.72}Co_{1.28}O_5(PO_4)_3$: (a) [001] (b) [100] experimental and schematically represented electron diffraction pattern. The patterns are indexed with a modulation vector $q^* = 1/2a^* + (1/3 + \varepsilon)b^*$. In the schematic representation of the pattern black points correspond to the basic spots, black crosses to the extinct basic spots, gray points to the modulation spots and gray crosses to the extinct modulation spots. Empty gray circles in (b) remain not explained with the modulation q^* and question the b-glide plane.

does not involve the $TT/DtDt$ sequence along c, but may picture tunnels cations, Bi^{3+}/M^{2+} edges of ribbons or PO_4 configurations ordering in the [110] plane.

[100] EDP (Fig. 11b): It is compatible with the q^* vector but supplementary weaker spots (schematically represented by gray empty circles) remain not explained with the modulation defined by q^*. These spots can be indexed in the basic cell as $0\,1\,l$, $l = 1, 3, 5\ldots$ and question the b-glide plane. It is to say that this symmetry is not perfectly respected at the crystallite scale while average effects make it available at the single crystal scale. To illustrate this feature, it is obvious that, depending on the explored volume, the presence of statistic disorder at the edges of ribbons may lead, either to the consideration of a unique Bi^{3+}/M^{2+} site with the conservation of the b-glide (single crystal case), either, in regard to a smaller number of unit cells, on to Bi^{3+} and M^{2+} distinction yielding the loss of this symmetry. Tunnels ordering may be involved since the b-glide relates two equivalent positions in the same tunnel, e.g., $0, y, 0$ and $0, y + \frac{1}{2}, 0$.

[010] ZAP: No extra spots are evidenced on the [010] ZAP in good agreement with both the modulation vector $q^* = 1/2a^* + (1/3 + \varepsilon)b^*$ (only third order spots should exist close to the observed plane but are expected very weak) and the b-glide disappearing.

5. Concluding remarks

The compounds described here can be formulated $[Bi_4Cd_4O_6]_2[Bi_2Cd_{3.44}Co_{0.56}O_4]_2Co_4(PO_4)_{12}$ taking account of its description in term of bidimensional polycationic ribbons surrounded by PO_4 groups and created tunnels. The novel nomenclature established, based on double, triple and tunnel arrangements allows to establish the ($TT/DtDt$) sequence for the title compounds. Furthermore, a number of previously described materials have been classified in respect to this nomenclature. The HREM/crystal structure correlation is informative since the strong contrast appearing between the ribbons framework and the disordered interzone enables an easy sequence determination. In the same way, new metal-oxyphosphates have been very recently isolated and studied. They are currently under investigation and will be presented in papers to come.

References

[1] J. Huang, A.W. Sleight, J. Solid State Chem. 100 (1992) 170.
[2] J. Huang, Q. Gu, A.W. Sleight, J. Solid State Chem. 105 (1993) 599.
[3] I. Radosavlejevic, J.S.O. Evans, A.W. Sleight, J. Solid State Chem. 137 (1993) 143.
[4] I. Radosavlejevic, J.S.O. Evans, A.W. Sleight, J. Solid State Chem. 141 (1998) 149.
[5] F. Abraham, O. Cousin, O. Mentre, El M. Ketatni, J. Solid State Chem. 167 (2002) 168.
[6] F. Abraham, M. Ketatni, Eur. J. Solid State Inorg. Chem. 32 (1995) 429.
[7] M. Ketatni, F. Abraham, O. Mentre, Solid State Sci. 1 (1999) 449.
[8] S. Nadir, J.S. Swinnea, H. Steinfink, J. Solid State Chem. 148 (1999) 295.
[9] X. Xun, S. Uma, A.W. Sleight, J. Alloys Compd. 1 (2002), in press.
[10] J. Huang, Q. Gu, A.W. Sleight, J. Solid State Chem. 105 (1993) 599.
[11] F. Abraham, M. Ketatni, G. Mairesse, B. Mernari, Eur. J. Solid State Chem. 31 (1994) 313.
[12] N. Tancret, Ph.D. dissertation, Université des Sciences et Technologies de Lille, France, Septembre 1995.
[13] A. Mizrahi, J.P. Wignacourt, H. Steinfink, J. Solid State Chem. 133 (1997) 516.
[14] A. Mizrahi, J.P. Wignacourt, M. Drache, P. Conflant, J. Mater. Chem. 5 (1995) 901.
[15] M. Ketatni, B. Mernari, F. Abraham, O. Mentre, J. Solid State Chem. 153 (2000) 48.
[16] S. Giraud, A. Mizrahi, M. Drache, P. Conflant, J.P. Wignacourt, H. Steinfink, Solid State Sci. 3 (2001) 593.
[17] F. Abraham, M. Ketatni, B. Mernari, Adv. Mater. Res. 1 (1994) 2.
[18] X. Xun, S. Uma, A.W. Sleight, J. Solid State Chem. (2002), in press.
[19] M. Ketatni, M. Huve, F. Abraham, O. Mentre, J. Solid State Chem. (2002), in press.
[20] JEMS—P.STADELMANN—1999–2003.
[21] "SAINT+" ver. 5.00, Bruker Analytical X-ray Systems, 2001.
[22] G.M. Sheldrick, SHELXTL NT ver. 5.1, Bruker analytical X-ray System, 1998.
[23] SADABS V2.03, Bruker/Siemens Area detector absorption and other corrections, 2001.
[24] V. Petricek, M. Dusek, JANA 2000, Institute of Physics, Praha, Czech Republic, 1997.
[25] O. Cousin, M. Huve, P. Roussel, O. Perez, H. Steinfink, J. Solid State Chem. 165 (2002) 324–333.
[26] F. Abraham, M.F. Debreuille-Gresse, G. Mairesse, G. Nowogrocki, Solid State Ionics 28–30 (1998) 529.
[27] F. Abraham, J.C. Boivin, G. Mairesse, G. Nowogrocki, Solid State Ionics 40–41 (1993) 934.
[28] J.P. Morniroli, J.W. Steeds, Ultramicroscopy 45 (1992) 219–239.